1 Analytical method

1.1 Mineral chemistry

To survey the textures and mineral para-genetic assemblages on thin sections of the samples, backscattered electron (BSE) imaging and quantitative elemental analyses of minerals were carried out by a JEOL JXA–8100 electron microprobe (EMP) at both the State Key Laboratory for Mineral Deposits Research (MiDeR), Nanjing University and Nanjing Hongchuang Geological Exploration Technology Service Co.

Quantitative elemental analyses of minerals were undertaken on polished thin sections using a JEOL JXA–8100 electron microprobe. The electron microprobe was operated with an accelerating voltage of 15 kV, a probe current of 20 nA, and an electron beam with a diameter of 1 μm (for feldspar, the diameter is 10 μm). All data were corrected using standard ZAF correction procedures.

Trace element analyses of minerals were conducted by LA–ICP–MS at the State Key Laboratory of Geological Processes and Mineral Resources, China University of Geosciences, Wuhan. Detailed operating conditions for the laser ablation system and the ICP–MS instrument and data reduction are the same as the description by Liu et al. (2008). Laser sampling was performed using a GeoLas Pro. An Agilent 7500a ICP–MS instrument was used to acquire ion–signal intensities. A “wire” signal smoothing device is included in this laser ablation system, by which smooth signals are produced even at very low laser repetition rates down to 1 Hz (Hu et al. 2012). Helium was applied as a carrier gas. Argon was used as the make–up gas and mixed with the carrier gas via a T-connector before entering the ICP. Nitrogen was added into the central gas flow (Ar+He) of the Ar plasma to decrease the detection limit and improve precision (Hu et al. 2008). Each analysis incorporated a background acquisition of approximately15–20 s (gas blank) followed by 50 s of data acquisition from the sample. The Agilent Chemstation was utilized for the acquisition of each individual analysis. Element contents were calibrated against multiple–reference materials (BCR-2G, BIR-1G, and BHVO-2G) without applying internal standardization, while GSE-1G, CGSG-1, and CGSG-2 were used for quality control (Liu et al. 2008). Every 8-sample analyses were followed by one analysis of NIST SRM 610 to correct the time-dependent drift of sensitivity and mass discrimination for the trace element analysis (Liu et al. 2008). All analyses were acquired using time-resolved software. Off-line selection and integration of background and analyte signals, and time-drift correction and quantitative calibration were performed by ICPMSDataCal (Liu et al. 2008; Liu et al. 2010a, b).

1.2 Laser Raman analyses

To characterize the composition of fluid inclusions, doubly polished thin sections (~100 μm) were prepared for Laser Raman analyses. Thirteen fluid inclusions from different charnockite samples were analyzed. These inclusions were selected because they form isolated inclusions or inclusion groups away from obviously healed micro-fractures. They thus represent the most probable candidates for fluid inclusions with primary composition. All data were collected at the State Key Laboratory for Mineral Deposits Research at Nanjing University, China, using a Renishaw-RM2000 Laser Raman Spectrometer with an Ar-ion laser and a surface power of 5 mW to supply the excitation radiation (514.5 nm). A charge-coupled device (CCD) of 20 area pixels was used as the detector, and the spectral scanning range was set to 1000–4000 cm^{-1} with an accumulation time of 60 s for each scan.

2 Timescale of the metamorphic overprint and element diffusion lengths of the Yunlu charnockite

The timescales of metamorphic thermal evolution could be constrained based on element diffusion profiles in garnets (Ague and Baxter, 2007). Thus, preservation of pre-existing chemical zoning of garnet constrains the timescales of thermal events, if diffusion rates, temperature, and initial concentration profiles are well constrained. We report on the results of diffusion modeling of compositional profiles on the Grt_1 rim from the Yunlu charnockite. If the initial conditions, boundary conditions and diffusion coefficient of the element of interest are known, the timescale can be obtained by fitting a model to the concentration profile. Boundary conditions control whether the crystal exchanges matter with its surroundings or not. The initial condition refers to the shape of the compositional profile before diffusion is considered.

In this study, the important assumptions regarding the suitable diffusion model, reasonable initial and boundary conditions and diffusion coefficient of the element of interest are necessary (Ague and Carlson 2013). Based on the rim composition of Grt_1, the time of diffusion was modelled from the Ca-diffusion profiles, which is most pronounced and thus most sensitive to variations in time. A planar source, infinite diffusion model (Costa and Morgan 2011; also named diffusion couple by Zhang 2010) is cited and the following analytical solution to the diffusion equation can be used:

$$\mathrm{C(x,t)} = C_s + \frac{(C_i - C_s)}{2}\,\mathrm{erfc}\,\frac{x}{2\sqrt{Dt}} \qquad (1)$$

Where erfc is the complementary error function, D is diffusion coefficient, t is diffusion time, C_i and

C_s are the initial concentration difference between the two sides of the couple, $C(x, t)$ is the concentration of element at position x (μm) and time t (Ma). The Equation (1) is applied only if (a) the compositions on either side of the diffusion zone are fixed, (b) the temperature and pressure for the entire time of diffusion is fixed. The initial and boundary conditions are given as follows:

Initial conditions: $t = 0$, $x > 0$, $C_s = 4.5$ mol%; $x < 0$, $C_i = 8.5$ mol%

Boundary conditions: $t > 0$, $x \rightarrow -\infty$, $C_i = 8.5$ mol%; $x \rightarrow \infty$, $C_s = 4.5$ mol%

As for the diffusion coefficient, we introduce the effective binary diffusion coefficient (EBDC, Cooper 1968) approach in order to simplify calculation, which is the most widely used simple treatment of diffusion in a multicomponent system. This method was developed to reduce the multicomponent diffusion problem to a pseudo-binary one, so that for a given component the entire solvent matrix behaves as a single component. In this approach, the diffusion of a component in a multicomponent system is treated as diffusion in a binary system, of which one is the component of interest and the other is interrelated component. The effective binary diffusion coefficient is expressed as follows:

$$D_{EBDC} = D_{AB} = \frac{D_A D_B (X_A + X_B)}{X_A D_A + X_B D_B} \{1 + \frac{d \ln \gamma_B}{d \ln X_B}\} \qquad (2)$$

where X_A and X_B are mole fractions of element A and B, and γ_B is the chemical activity coefficient of component B. D_A and D_B are the diffusion coefficient of element A and B, respectively. In practice, the $\frac{d \ln \gamma_B}{d \ln X_B}$ is near zero and could be ignored. Therefore, the equation (2) can be simplified as follows:

$$D_{EBDC} = D_{AB} = \frac{D_A D_B (X_A + X_B)}{X_A D_A + X_B D_B} \qquad (3)$$

In view of the diffusion coefficient of Ca is tightly correlated with Fe in garnet (Chu and Ague 2015), we use the Fe-Ca interdiffusion coefficient to represent the effective binary diffusion coefficient. The equation (3) can be shown as below:

$$D_{EBDC} = D_{Ca-Fe} = \frac{D_{Ca} D_{Fe} (X_{Ca} + X_{Fe})}{X_{Ca} D_{Ca} + X_{Fe} D_{Fe}} \qquad (4)$$

The diffusion coefficient of Ca and Fe in garnet are listed in Table S1. The modeling results are shown on Fig. 11a. Diffusional modelling of the Ca-diffusion profile of Grt_1 provides a maximal duration estimate of the metamorphic pulse with ~ 0.5 Ma.

Based on the duration of the thermal pulse/peak and diffusion coefficient of elements at given temperature, we can quantitatively estimate the influence of element re-equilibrium of mineral

compositions by intra -crystalline cation diffusion. If we assume the temperature and timescale of the metamorphic thermal pulse is 750 °C and 0.5 Ma, respectively. Then we can estimate the one-dimension diffusion lengths/distances of various elements in different minerals according to the following formula:

$$L = \sqrt{D * t} \qquad (5)$$

Where the L is the diffusion length, D is the diffusion coefficient which is chiefly controlled by temperature and t is the time. The various element diffusion coefficient in different minerals are listed on Table S1. Considering the orthopyroxene-garnet, garnet-biotite and orthopyroxene-biotite thermometer are based on Fe-Mg exchange equilibria between two minerals primarily, the influence of Fe-Mg inter-diffusion are estimated. For the two-feldspar thermometer, it is based on ternary feldspar equilibria between plagioclase and K-feldspar. Hence, both influences of NaSi-CaAl inter-diffusion in plagioclase and Na-K inter-diffusion in K-feldspar are evaluated. The Fe-Mg inter-diffusion coefficient in biotite is depend on the crystallographic orientation that is adjacent to interface with garnet and orthopyroxene, slow diffusivity parallel to the (001) axis (similar to Fe-Mg inter-diffusion in garnet) and much faster diffusivity perpendicular to it. (Usuki 2002). Therefore, only the biotite grains that are parallel to the garnet or orthopyroxene are chosen to calculate the temperature. The calculated diffusion lengths are shown on Fig. 11b. The Fe-Mg inter-diffusion lengths of biotite, garnet and orthopyroxene at 0.5 Ma and 750 °C are less than 100 μm (Fig. 11). While the NaSi-CaAl inter-diffusion length in plagioclase and Na-K inter-diffusion length in K-feldspar are <1 μm and ~4 mm, respectively.

Table S1. Element diffusion coefficient in different minerals at 750 °C.

Mineral	Diffusion coefficient (D) (m^2/s) at 750 °C	Reference
Fe-Mg inter-diffusion in Opx (D_{Fe-Mg}^{Opx})	$10^{-21.5}$	Cherniak and Diamnov 2010; Dohmen 2016
Fe-Mg inter-diffusion in Bt (D_{Fe-Mg}^{Bt})	10^{-22}	Usuki 2002
Fe-Mg inter-diffusion in Grt (D_{Fe-Mg}^{Grt})	10^{-22}	Carlson 2006; Chu and Ague 2015
Ca diffusion in Grt (D_{Ca}^{Grt})	10^{-23}	Carlson 2006; Chu and Ague 2015

Fe diffusion in Grt (D_{Fe}^{Grt})	10^{-22}	Carlson 2006; Chu and Ague 2015
NaSi-CaAl inter-diffusion in Pl ($D_{NaSi-CaAl}^{Pl}$)	10^{-26}	Cherniak 2010
Na-K inter-diffusion in Kfs (D_{Na-K}^{Kfs})	10^{-18}	Cherniak 2010

3 Geochemical modeling of crystallization-differentiation process in the Yunlu charnockite

To accurately constrain the crystallization-differentiation of the Yunlu charnockite, we employ the in-situ crystallization model which better captures the fractional process in silicic magma chamber. The physical model of our calculations is similar to that of Langmuir (1989) and the calculation procedures are the same as the methods described in Zhao et al (2018). But we make following modifications in this study to better capture the geochemical characteristics of the Yunlu charnockite. (a) We cease the calculation when the modeled cumulate pile compositions match the most felsic charnockite sample rather than the calculated residual magma composition matched that of the most felsic Opx-free granite. (b) Interstitial melt was assumed to be extracted at a critical crystallinity of 0.4 instead of 0.5 (Bachmann and Bergantz, 2004) and the melt fraction at this crystallinity was modelled to have been extracted from solidification zone. (c) The compositions of interstitial melt are those determined by the thermodynamic modeling. The melt composition that we have used for constraining the evolution of the solidification zones is yielded by rhyolite-MELTS modeling using the different initial composition, i.e. by determining the melt composition at the critical crystallinity (CC = 0.4).

The geochemical modeling requires an initial composition as an input parameter. Two samples with different initial compositions are considered. The sample D19-4 that is used for thermodynamic modeling in section xx is considered as one of the initial compositions as well. Due to all the Yunlu charnockite samples (including D19-4) experience melt extraction and are cumulate. Hence, we also synthetize a sample MC01 as an initial composition. The chemical composition of MC01 consists of 60% charnockite 15GZ19 and 40% interstitial melt in order to offset the effect of fractional crystallization. The sample 15GZ19 is the most mafic charnockite in Yunlu pluton (Appendix Table 3) and the interstitial melt composition is cited from White and Chappell (1974) (Appendix Table 5). The model was run step by step in 7-9 increments to approximate continuous fractionation based on various initial compositions. At each increment, 0.2 of the magma masses (Hertogen and Mareels, 2016) was crystallized in a solidification zone until the composition of the cumulate pile matched that of the most

felsic charnockite. The interstitial, unextracted melt fraction of our numerical model was then set to 10% for the first solidification zone and it was increased by 2% for each of the subsequently modelled solidification fronts to account for the estimated range of unextracted interstitial melt. The concept of the model is similar as Zhao et al. (2018), while all modeling results are reported in Appendix Table 5 and shown on Fig. 8.

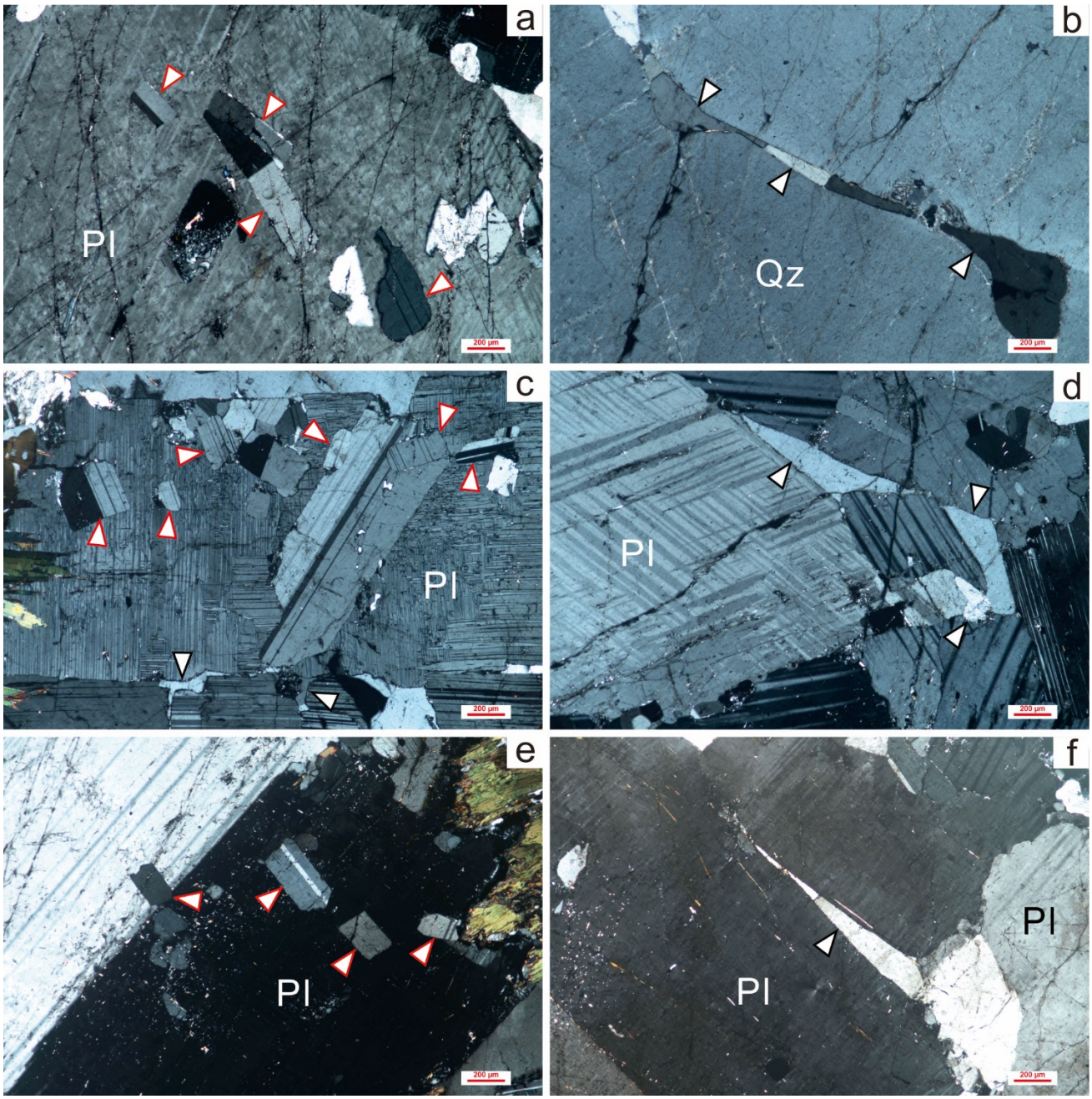

Fig. S1. (a), **(c)** and **(e)**: The euhedral to subhedral, tabular plagioclase inclusions are enclosed in large euhedral plagioclase crystals, indicated by arrow with red rim. The crystal faces of plagioclase inclusions against large plagioclase crystals, showing no evidence of grain-shape changes during later metamorphic overprint. Crossed polars. **(b)**, **(d)** and **(f)**: The quartz crystals showing an irregular film

(arrow with black rim) separating quartz (b) or plagioclase crystals (d and f). Such a feature suggests that quartz infilled a grain-boundary melt film with irregular margins. Crossed polars.

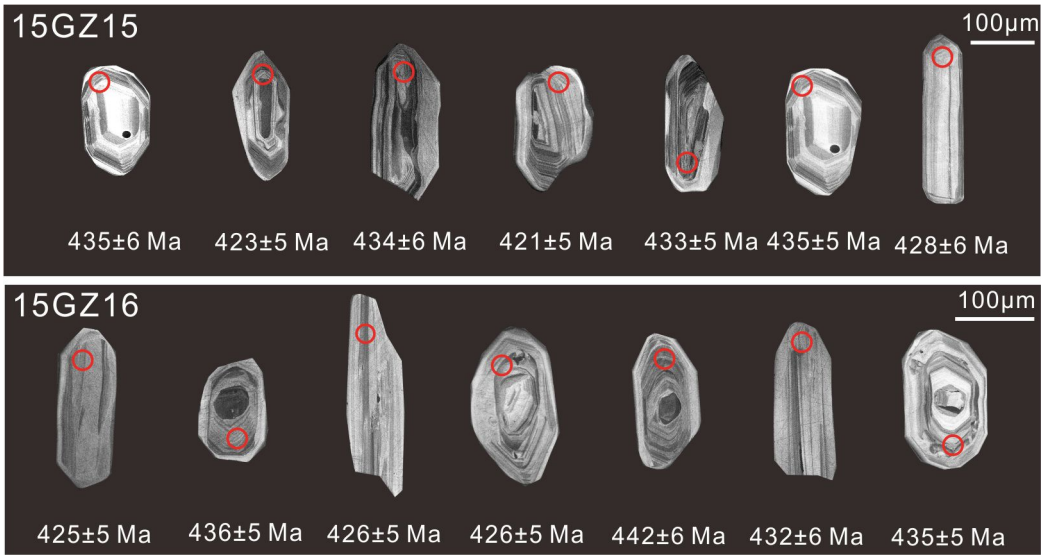

Fig. S2. CL images and U-Pb geochronology results of representative zircon from Yunlu charnockite. Red solid circles are spots for U-Pb isotope analyses.

References cited

Ague, J. J., and Baxter, E.F. (2007). Brief thermal pulses during mountain building recorded by Sr diffusion in apatite and multicomponent diffusion in garnet. Earth and Planetary Science Letters, 261, 500–516.

Ague, J. J. and Carlson, W.D. (2013). Metamorphism as garnet sees it: the kinetics of nucleation and growth, equilibration, and diffusion relaxation. Elements, 9, 439–445.

Carlson, W.D. (2006) Rates of Fe, Mg, Mn, and Ca diffusion in garnet. American Mineralogist, 91:1–11.

Cherniak, D.J., and Dimanov, A. (2010) Diffusion in pyroxene, mica and amphibole. Reviews in Mineralogy and Geochemistry, 72, 641–690.

Cherniak., D.J. (2010) Cation diffusion in feldspars. Reviews in Mineralogy and Geochemistry, 72:691-734.

Chu, X., and Ague, J.J. (2015) Analysis of experimental data on divalent cation diffusion kinetics in aluminosilicate garnets with application to timescales of peak Barro-vian metamorphism, Scotland. Contributions to Mineralogy and Petrology, 170, 1–27.

Costa, F., and Morgan, D. (2011) Time Constraints from Chemical Equilibration in Magmatic Crystals

(*In:* Timescales of Magmatic Processes: From Core to Atmosphere) 125–159.

Cooper, A.R. (1968) The use and limitations of the concept of an effective binary diffusion coefficient for multicomponent diffusion. *In:* Mass Transport in Oxides, Vol 296. Wachman JB, Franklin AD (eds) Nat Bur Stand Spec Publ, p 79-84.

Dohmen, R., Ter Heege, J.H., Becker, H.-W., and Chakraborty, S., (2016) Fe–Mg inter-diffusion in orthopyroxene. American Mineralogist,101, 2210–2221.

Hu, Z.C., Gao, S., and Liu, Y.S. (2008) Signal enhancement in laser ablation ICP-MS by addition of nitrogen in the central channel gas. Journal of Analytical and Atomic Spectrometry, 23, 1093-1101.

Hu, Z.C., Liu, Y.S., Gao, S., Liu, W., Zhang, W., Tong, X., Lin, L., Zong, K.Q., Li, M., Chen, H., Zhou, L., and Yang, L., (2012) Improved in situ Hf isotope ratio analysis of zircon using newly designed X skimmer cone and jet sample cone in combination with the addition of nitrogen by laser ablation multiple collector ICP-MS. Journal of Analytical Atomic Spectrometry, 27(9), 1391-1399.

Liu, Y.S., Hu, Z.C., Gao, S., Günther, D., Xu, J., Gao, C., and Chen, H. (2008) In situ analysis of major and trace elements of anhydrous minerals by LA-ICP-MS without applying an internal standard. Chemical Geology, 257(1–2), 34-43.

Liu, Y.S., Gao, S., Hu, Z.C., Gao, C.G., Zong, K.Q., and Wang, D.B., (2010a) Continental and oceanic crust recycling-induced melt-peridotite interactions in the Trans-North China Orogen: U-Pb dating, Hf isotopes and trace elements in zircons of mantle xenoliths. Journal of Petrology, 51(1-2), 537-571.

Liu, Y.S., Hu, Z.C., Zong, K.Q., Gao, C.G., Gao, S., Xu, J., and Chen, H.H. (2010b) Re-appraisement and refinement of zircon U–Pb isotope and trace element analyses by LA-ICP-MS. Chinese Science Bulletin, 55, 1535–1546.

Uzuki., T. (2002) Anisotropic Fe–Mg diffusion in biotite. American Mineralogist, 87, 1014–1017.

Zhang, Y., and Cherniak, D.J. (2010) Diffusion in minerals and melts: Theoretical background. Reviews in Mineralogy and Geochemistry, 72, 5–60.